# In-Vessel Storage Cooling Analysis in PGSFR

Jung Yoon [a*], Tae-ho Lee [a]
[a] *Korea Atomic Energy Research Institute, Fast Reactor Development Div., 1045 Daedeok-daero, Daejeon*
[*] *Corresponding author: jyoon@kaeri.re.kr*

## 1. Introduction

The thermal-hydraulics of the RV inside is very important in the design of a PGSFR. One of various design issues related to this region is the thermal-hydraulic behavior of an In-Vessel Storage (IVS) to store the spent fuel. The IVS is the place where store the spent fuel temporarily. It is located in the annular space of the reactor core outside, and the spent fuel is stored for two cycles in IVS to reduce the decay heat and radioactivity. A total of 60 spent fuel can be stored in IVS, the minimum distance between spent fuels is more than 20 mm. The spent fuel is fixed in such a way that the nose piece is mounted on the receptacle, which is the same way as the core.

Since the spent fuel stored in IVS generates the decay heat continuously, it is necessary to cool the spent fuel during the storage period. However, it is not possible to cool the spent fuel by using cold sodium in the inlet plenum because the orifice hole in the receptacle is blocked.

In this study, the cooling performance of spent fuels in IVS by the natural convection due to the temperature difference between hot pool and IVS inside using CFD is assessed.

## 2. Methods and Results

### *2.1 Heat source determination*

ANS standard decay heat power [1] is referred to simulate the decay heat of spent fuel after 48 hours. This value is used as the heat source of the bundle region. The decay heat curve over time is shown in Figure 1.

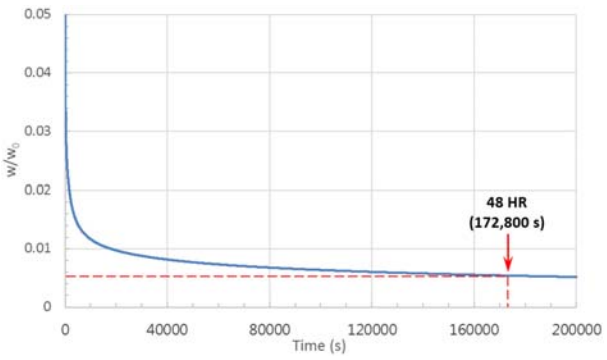


Fig. 1. Decay heat curve over time

### *2.2 1-D lumped parameter study*

Prior to the CFD analysis, 1-D lumped parameter analysis [2] based on simple momentum and energy balance equations to calculate the flow behavior and assembly heat-up under 1-D natural convection flow conditions is performed. The analysis is performed about one FA, and heat transfer from the FA to the surrounding sodium inside IVS is neglected. Also, these results are compared with CFD results in same boundary conditions. Detail geometry and boundary condition are shown in Figure 2, and assumptions for analysis are shown as follows.

- Flow inside IVS and FA is generated by natural convection only
- Conjugate heat transfer through FA duct is not considered
- IVS wall is adiabatic
- Bundle region is treated as porous media, and the pressure drop in normal operating condition is applied
- Decay heat is generated in whole bundle region
- Peak fuel cladding temperature is defined as below

$$T_{f,max} = T_{Na,exit} + \frac{\dot{Q}R_f^2}{2k_c}\left\{ln\left(\frac{R_c}{R_f}\right) + \frac{k_c}{2k_f} + \frac{k_c}{h_{con}R_c}\right\}$$

Where, $T_{Na,exit}$ : FA exit temperature
$\dot{Q}$ : Fuel volumetric power density
$R_f$, $R_c$ : Fuel and cladding radius
$k_f$, $k_c$ : Fuel and cladding conductivity
$h_{con}$ : Convective heat transfer coefficient

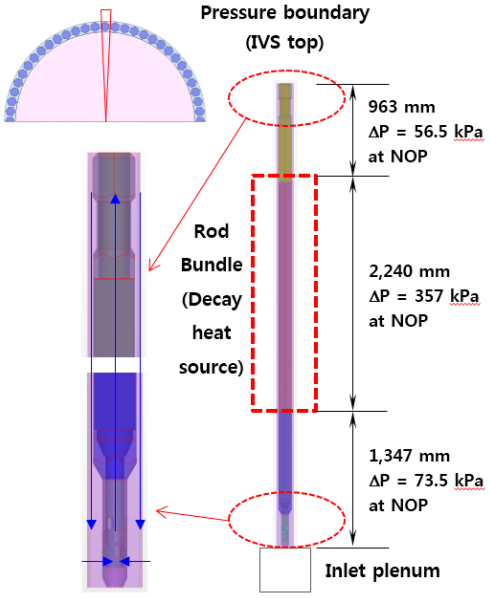


Fig. 2. IVS cooling analysis domain and boundary condition

A CFD analysis is performed by STAR-CCM+ V9.02.007. A three-dimensional, and steady-state flow is assumed. Material properties such as the density, viscosity, specific heat and conductivity are given as a function of temperature [3]. Also, the realizable $k-\epsilon$ turbulence model is used. The total number of computational grids are 700,000 and this grid level is evaluated by the grid sensitivity test [4].

The geometry for CFD is same as the real spent fuel geometry, but FA inside regions are treated as porous media to satisfy the pressure loss requirements of normal operating condition because of geometrical complexity of bundle region and calculation time. Also, uniform decay heat source at 48 hours is assigned to whole bundle region. CFD result is compared with 1-D lumped parameter analysis and showed almost same result. Detailed results comparison between 1-D lumped parameter study and CFD are shown in Table 1.

Table 1. Comparison between CFD and 1-D analysis

| | Decay heat | Sodium velocity | | Peak fuel cladding temp. | Sodium temp. at FA exit | Bundle dP |
|---|---|---|---|---|---|---|
| | | Rod bundle | IVS inlet | | | |
| CFD | 19kW | 5.9 cm/s | 2.5 cm/s | 584.9℃ | 584.5 ℃ | 351Pa |
| 1-D | ~20 kW | ~11 cm/s | ~11 cm/s | ~585℃ | ~585℃ | - |

### *2.3 CFD analysis considering conjugate heat transfer*

Section 2.2 is evaluated only the effects of natural convection without the conjugate heat transfer through FA duct. In this section, the IVS cooling performance with the conjugate heat transfer through FA duct is evaluated. Assumptions for analysis are shown as follows.

- Conjugate heat transfer through FA duct is considered
- Other conditions are all same as section 2.2

Detailed results comparison between adiabatic and conjugate heat transfer case are shown in Table 2. Heat transfer from FA to gap diminishes natural convection downward flow along the annular gap. Also, complicated flow pattern is found in the annular gap and FA inside due to the decay heat transferred by the FA inside through the HT9 as shown in Figure 3. Although the flow through FA decreases, the average sodium temperature at FA exit decrease by the conjugate heat transfer. Also, it seems that overall flow pattern has transient characteristics. Detailed flow and temperature distributions are shown in Figure 4 and 5.

Table 2. Comparison between adiabatic and CHT

| Method | Average sodium flow velocity | | Avg. Sodium temp. at FA exit |
|---|---|---|---|
| | Rod bundle (FA exit) | Annular gap (inlet) | |
| Adiabatic | 5.9 cm/s | 2.5 cm/s | 584.5 ℃ |
| CHT | 4.2 cm/s | 1.8 cm/s | 580.5 ℃ |

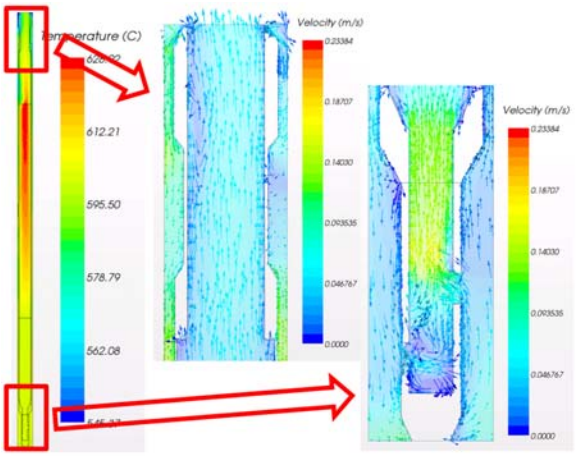


Fig. 3. Temperature and velocity distribution (CHT)

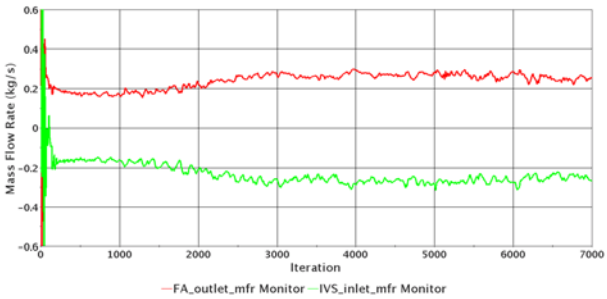


Fig. 4. Mass flow rate distribution over iteration (CHT)

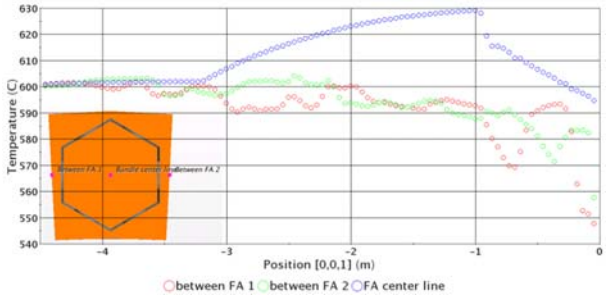


Fig. 5. Temperature distribution at FA center line (CHT)

### *2.4 CFD analysis considering real flow resistance*

For convenience of analysis, the bundle region in FA is treated as porous media, and the pressure drop in normal operating condition is applied. However, this approach is not appropriate because flow generated by natural convection in IVS is very low. Therefore, it is necessary to define a porous media using the resistance coefficient at low flow. In this section, the IVS cooling performance using the resistance coefficient at flow in normal operating condition and low flow is evaluated. Detail geometry and boundary condition are shown in Figure 6, and assumptions for analysis are shown as follows.

- Pressure drop in active bundle region uses the value at low flow, and pressure drop in other bundle region uses the value at normal operating condition
- Decay heat is generated only from the active bundle region
- Other conditions are all same as section 2.3

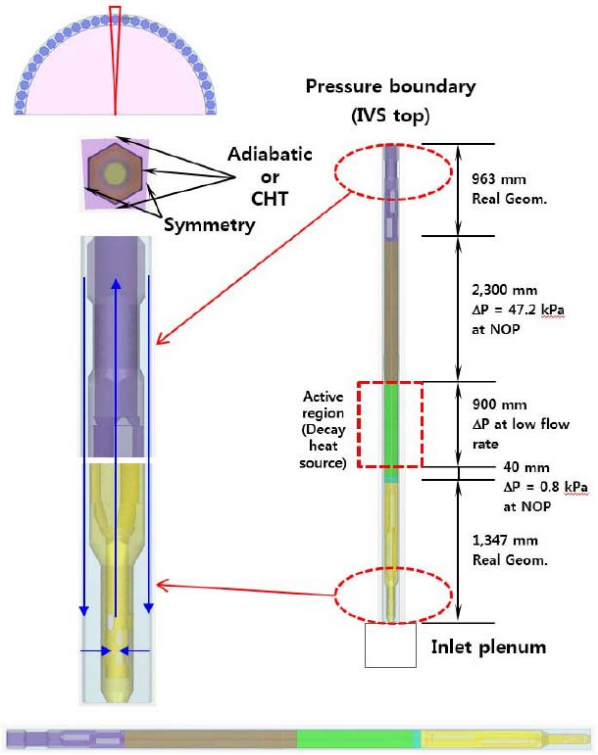


Fig. 6. IVS cooling analysis domain and boundary condition considering the flow resistance at low flow

To determine the resistance coefficient at low flow, CFD analysis for active bundle region only is performed. These results are compared to the pressure drop in low flow calculated by the SLTHEN code which is used in the core pressure drop calculation, and the resistance coefficient of porous media is adjusted accordingly. The flow – resistance coefficient table acquired through this process is shown in Table 3. The resistance coefficient in the flow rate calculated at first iteration is determined by linear interpolation function, and this value is used in next iteration.

Table 3. Pressure drop and resistance coefficient over flow rate

| Flow rate (kg/s) | Pressure drop (Pa) | Resistance coefficient ($kg/m^4$) |
|---|---|---|
| 0.1 | 18.88 | 1,287,380 |
| 0.2 | 71.86 | 512,859 |
| 0.4 | 241.72 | 280,835 |
| 0.6 | 491.45 | 224,579 |
| 0.8 | 813.05 | 198,610 |
| 1.0 | 1201.46 | 182,989 |

Detailed results comparison according to the difference of flow resistance are shown in Table 4. Flow rate of case 1 is smaller than case 2. Accordingly, the temperature at the active bundle outlet is more increased. However, the temperature at FA exit is more decreased due to the increase of heat loss toward annular gap. Detailed flow and temperature distributions are shown in Figure 7 ~ 9.

Table 4. Comparison of different resistance coefficients

| | Resistance coef. | Mass flow rate (avg.) | Avg. Sodium temp. | |
|---|---|---|---|---|
| | | | FA exit | Active bundle exit |
| Case 1 | Constant | 0.263 kg/s | 594.5 ℃ | 630.0 ℃ |
| Case 2 | Change to flow rate | 0.164 kg/s | 584.0 ℃ | 680.0 ℃ |

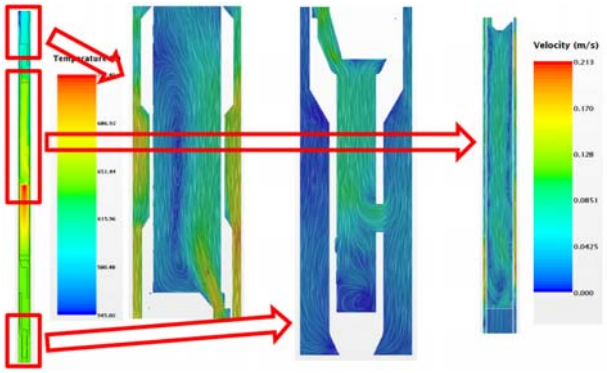


Fig. 7. Temperature and velocity distribution (Case 2)

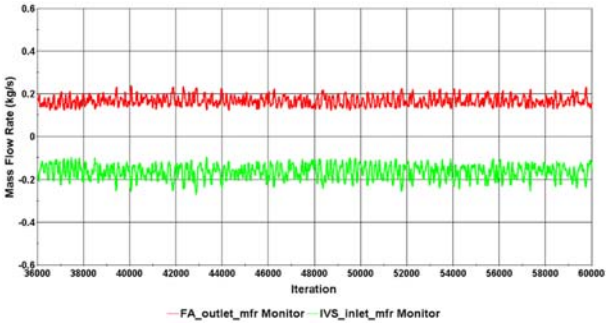


Fig. 8. Mass flow rate distribution over iteration (Case 2)

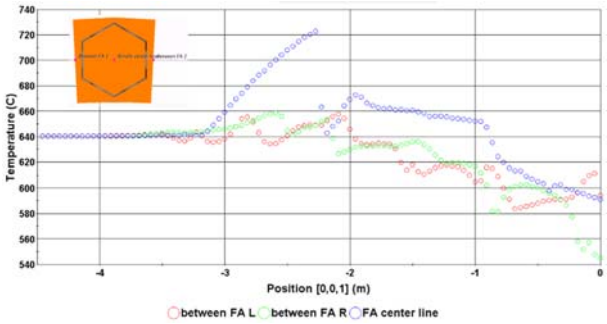


Fig. 9. Temperature distribution at FA center line (Case 2)

### *2.5 CFD analysis considering real geometry of the pool inside*

Results mentioned above are not considered the influence of the IVS outside because IVS inner and outer walls are adiabatic. Actually, there is the heat transfer between IVS and core (or cold pool), and this affects the temperature distribution in the IVS inside. For a more realistic analysis, the real geometry which has core, shielding, and cold pool is used for the cooling analysis. Detail geometry and boundary condition are shown in

Figure 10, and assumptions for analysis are shown as follows.

- The conjugate heat transfer in the wall adjacent to the core and cold pool is considered
- RV wall is adiabatic
- The core region is treated as porous media to satisfy the pressure loss requirements of normal operating condition
- The top and bottom walls of cold pool are adiabatic, and the initial temperature condition of cold pool is 390 ºC

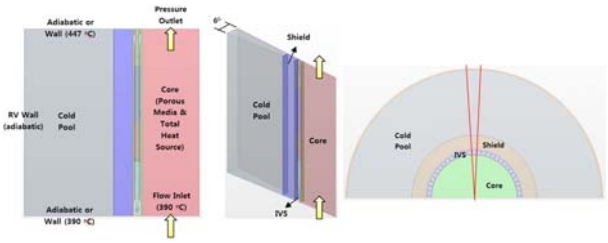


Fig. 10. IVS cooling analysis domain and boundary condition considering real geometry

Table 5. Comparison between IVS only and whole pool

| | Mass flow (kg/s) | Avg. Sodium temp. (℃) | | | Heat transfer (kW) | |
|---|---|---|---|---|---|---|
| | | FA exit | Active bundle exit | $dT_{IVS}$ | To cold pool | To core |
| Case 1 (IVS only) | 0.164 | 584.0 | 680.0 | 39.0 | - | - |
| Case 1-1 | 0.090 | 549.0 | 591.0 | 4.0 | 4.08 | 14.32 |

Detailed results comparison according to the geometry difference are shown in Table 5. The temperature in IVS inside of case 2 is more decreased than that of case 1 because of the heat transfer to the core and cold pool. For this reason, the temperature difference between IVS inlet and outlet is decreased, and the flow generated by natural convection is decreased. Also, the heat transfer to the core is bigger than that to the cold pool due to the shielding structure. Detailed flow and temperature distributions are shown in Figure 11 ~ 13.

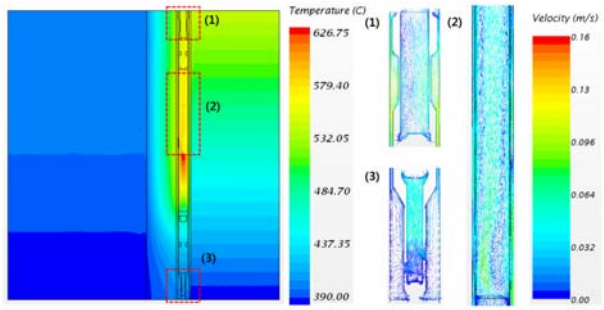


Fig. 11. Temperature and velocity distribution (Case 1-1)

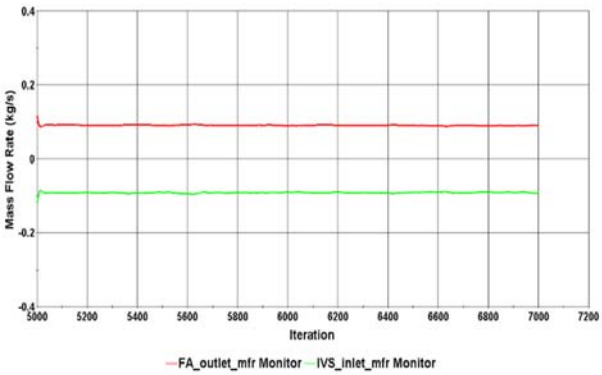


Fig. 12. Mass flow rate distribution over iteration (Case 1-1)

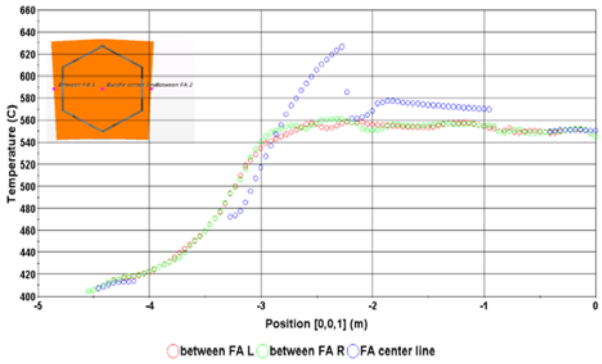


Fig. 13. Temperature distribution at FA center line (Case 1-1)

## 3. Conclusions

The IVS cooling performance analysis using natural convection due to the temperature difference between the IVS and hot pool is evaluated by CFD. The analyses in various geometry and boundary condition are performed. For all cases, the temperature at the active bundle outlet is higher than 590 ºC. Therefore, the spent fuel cooling in IVS using natural convection is difficult to expect the cooling effect.

## 4. Acknowledgement

This work was supported by the National Research Foundation of Korea (NRF) grant funded by the Korean government (MSIP). (No. 2012M2A8A2025624)

## REFERENCES

[1] American National Standards Institute, “American National Standard for Decay Heat Power in Light Water Reactors”, ANSI/ANS 5.1, 1979.
[2] M.T. Farmer, “In-Vessel Fuel Storage”, KAERI-ANL Joint Project Meeting, 2014.
[3] J. Yoon, Thermal-hydraulic Analysis report for PGSFR, KAERI, 2014.
[4] J. Yoon, IVS Thermal-hydraulic Analysis report, KAERI, 2014.